DOI: 10.1002/ejic.200500729

Theoretical Studies on Metal–Metal Interaction and Intrinsic ^{1,3}[σ*(d)σ(s/p)] Excited States of Dinuclear d^{10} Complexes with Bridging Phosphane Ligands

Qing-Jiang Pan,[a,b] Hong-Xing Zhang,*[a] Hong-Gang Fu,[b] and Hai-Tao Yu[b]

Keywords: Metallophilicity / Excited states / Dinuclear d^{10} complexes / Electronic structure / Solvent effects

To explore the metal–metal interaction and spectroscopic properties, the ground- and excited-state structures of $[M_2(dpm)_2]^{2+}$ [M = Ag (**2**), Cu (**3**), dpm = bis(diphosphanyl)-methane] and their solvated species $[M_2(dpm)_2]^{2+}\cdot(MeCN)_2$ were optimized by the MP2 and CIS methods, respectively. In the ground states, the calculated M–M distances and their corresponding M–M stretching frequencies for **2** and **3** indicate the presence of metallophilic attraction; there is strong N→Cu/Ag coordination in acetonitrile, which is different from the case in previous studies of $[Au_2(dpm)_2]^{2+}$ (**1**). CIS calculations show that **2** and **3** have $^{1,3}[\sigma^*(d)\sigma(s/p)]$ as their lowest-energy excited state, as is also the case for **1**, confirmed by unrestricted MP2 calculations. On the basis of the CIS-optimized structures, the TD-DFT (B3LYP) method was employed to calculate the emission spectra of such complexes. For **3**, the phosphorescent emissions were calculated at 424 and 514 nm in the solid state and acetonitrile, which is comparable to the experimental data of 475 and 480 nm, respectively. The comparison between the gas-phase and solution emissions for **1**–**3** reveals that the N→M coordination results in a large red-shift of the emission wavelength. Taking previous studies into account , we found that the M–M distances are linearly correlated with the M–M stretching frequencies for the dinuclear d^{10} complexes.

Introduction

Despite the fact that two closed-shell metal cations would normally be expected to repel each other, a larger number of inorganic and organometallic complexes have been described whose structures indicate strong metal–metal interactions.[1–5] Among these interactions, the Au^{I}–Au^{I} interaction has been intensively investigated both experimentally[6–11] and theoretically,[2–4,12–17] and coined as "aurophilicity" by Schmidbaur.[18] The energy of the aurophilic attraction in the solid state and solution was estimated to be 7–15 kcal/mol,[3] comparable to that of hydrogen bonds. Pyykkö et al.[1–4] have attributed the attraction to correlation effects that are strengthened by relativistic effects.

The Au–Au aurophilic attractions often result in unusual photochemical and photophysical properties for the Au^{I} complexes.[6–11] It was found that their unique spectroscopic features in the absorption and emission spectra clearly relate to the presence of the Au–Au interactions. The luminescence of Au^{I} complexes was assigned as a metal-centered (MC) transition or a metal–metal-to-ligand charge-transfer (MMLCT) transition.[12–17] Recently, we calculated the aurophilic interactions and excited-state properties of model complexes $[Au_2(dpm)_2]^{2+}$ (**1**),[12,13] $[Au_2(dpm)(i\text{-}mnt)]$ (**4**),[16] and $[(AuPH_3)_2(i\text{-}mnt)]$ (**5**)[16,17] [dpm = bis(diphosphanyl)-methane and i-mnt = i-malononitriledithiolate]. The results revealed that the 507-nm phosphorescent emission of **1** in acetonitrile has the σ[s(Au$_2$)]→σ*[d(Au$_2$)] (MC) transition property,[13] while the 512 and 495-nm emissions in the CH_2Cl_2 solution for **4** and **5**, respectively, arise from the Au–Au to i-mnt charge-transfer (MMLCT) transition.[16] The Au^{I}–Au^{I} interaction is strengthened in these emissive excited states, resulting from the formation of a σ single bond between the Au^{I} centers upon excitation.

Though aurophilic attraction between gold(I) atoms is widely acknowledged,[1–20] the development of silver–silver (argentophilicity)[21,22] and copper–copper (cuprophilicity)[22–24] bonding interactions remains in its infancy. Che and coworkers[25–32] have structurally characterized a series of luminescent dinuclear d^{10} complexes with bridging phosphane ligands. The d^{10}–d^{10} metallophilicity in these complexes was confirmed by Raman spectroscopy. For $[M_2(dcpm)_2](X)_2$ [M = Au, Ag, and Cu; X = counteranion; dcpm = bis(dicyclohexylphosphanyl)methane], with metal–metal distances of 2.939, 2.960, and 2.731 Å, respectively, the 88, 80, and 104-cm^{-1} fundamental bands were assigned to the M–M stretching vibrations.[27–29] These d^{10} complexes exhibit intense luminescence either in the solid state or in solution, which is experimentally attributed to the σ[(*n* + 1)p]→σ*(*n*d) transitions.

Apart from the above fundamental interest, the existing and/or potential applications based on d^{10} coinage metal

[a] State Key Laboratory of Theoretical and Computational Chemistry, Institute of Theoretical Chemistry, Jilin University, Changchun 130023, China
[b] College of Chemistry and Chemical Engineering, Heilongjiang University, Haerbin 150080, China
Supporting information for this article is available on the WWW under http://www.eurjic.org or from the author.

complexes such as optical materials, photocatalysts, biosensors, and molecular pharmacology have also received the attention of many researchers.[6,22–24,33–37] For example, it has been suggested that the therapeutic action of gold drugs for rheumatoid arthritis is related to the ability of the Au^I complexes to quench the singlet oxygen $^1\Delta_g$ state at 7752 cm^{-1}.[37] Such applications of the d^{10} complexes are clearly pertinent to their excited-state properties. Therefore, the theoretical investigation of the electronic structures of the ground- and excited states of the complexes is also of practical significance.

So far, computational methods are sufficiently advanced to allow calculation of ground- and excited states of relatively large molecular complexes.[38] At the same time, experiments provide wide and accurate information that can serve as a test for the computational methods. In theory these make both the systematic investigations of the M–M interactions and the luminescence of the d^{10} coinage metal complexes possible. Since the presence of a bridging ligand facilitates the intramolecular interaction,[4] the series of complexes, $[M_2(P–P)_2]^{2+}$ [M = Au, Ag, and Cu; P–P = dmpm, dppm, and dcpm; dmpm = bis(dimethylphosphanyl)methane and dppm = bis(diphenylphosphanyl)methane], with eight-membered-ring conformation,[24–31,38–44] are ideal candidates for such investigations.

Here, we use the second-order Møller–Plesset perturbation (MP2)[46] and single excitation configuration interaction (CIS)[38] methods to fully optimize the ground- and excited-state structures of model complexes $[M_2(dpm)_2]^{2+}$ [M = Ag (**2**) and Cu (**3**)] and their solvated species $[M_2(dpm)_2]^{2+}\cdot(MeCN)_2$, respectively. On the basis of the MP2- and CIS-optimized structures, the absorption and emission spectra of such complexes were obtained from TD-DFT (time-dependent density functional theory)[47–49] calculations, respectively. Combined with the previous studies on **1**, the calculated M–M distances (3.03–3.16 Å) and their corresponding M–M stretching frequencies (69–89 cm^{-1}) for **1**–**3** indicate the presence of metallophilic attraction in the ground states. Complexes **1**–**3** give rise to the metal-centered $\sigma(s, p_z)\rightarrow\sigma^*(d_{x^2-z^2}, d_{y^2})$ emissions, both in the gas phase and in solution, revealing that the dinuclear d^{10} complexes with bridging phosphane ligands have the intrinsic $^{1,3}[\sigma^*(d)\sigma(s/p)]$ excited states (the M_2P_4 unit lies in the *xz* plane and the *z* axis goes through the two metal atoms).

Computational Details and Theory

It has been found that the complexes, $[M_2(P–P)_2]^{2+}$ (M = Au, Ag, and Cu; P–P = dmpm, dppm, and dcpm), form a series of discrete dinuclear M(I) dimers in the crystalline phase, i.e. no intermolecular M(I)–M(I) interactions.[25–30,40–45] There are close cation–anion contacts of 2.692 and 2.687 Å (M···O) in the crystal lattices of $[Ag_2(dcpm)_2]\cdot(CF_3SO_3)_2$[28] and $[Cu_2(dcpm)_2]\cdot(ClO_4)_2$,[29] respectively, but such interactions are not apparent in the X-ray structure of the gold(I) congener $[Au_2(dcpm)_2]\cdot(ClO_4)_2$ (closest Au···$OClO_3$, 3.362 Å).[25,26] Therefore, these types of complexes can be modeled by $[M_2(dpm)_2]^{2+}$ and $[M_2(dpm)_2]\cdot(ClO)_2$, which reflect the behaviors in the gas phase and solid state, respectively. To save the computational resources, the hydrogen was used to replace methyl, phenyl, cyclohexyl and other heavy substituents in the ab initio studies. A similar model has been applied in many studies.[12–17,50,51]

In this work, we employed the C_i symmetry to settle the ground- and excited-state conformations of $[M_2(dpm)_2]^{2+}$ [M = Ag (**2**) and Cu (**3**)], which are consistent with the results from the X-ray diffraction study of $[M_2(dcpm)_2]\cdot(X)_2$ (X = counteranion).[28–30] Because the solvent affects the luminescence of the complexes,[12,13,16,17,25–32,40] we used the solvated species $[M_2(dpm)_2]^{2+}\cdot(MeCN)_2$ to establish the solvent effects of acetonitrile.

All the calculations were carried out using the GAUSSIAN03 program package.[52] The ground- and excited-state structures of **2** and **3** and their solvated species were fully optimized by the MP2[46] and CIS[38] methods, respectively. On the basis of such optimized structures, the TD-DFT (B3LYP)[47–49] method was performed to calculate the absorption and emission spectra of the complexes.

In the calculations, quasi-relativistic pseudopotentials of the Ag, Cu, and P atoms proposed by Hay and Wadt[53,54] with 19, 19, and 5 valence electrons, respectively, were employed, and the LanL2DZ basis sets associated with the pseudopotential were adopted. In order to describe the d^{10}–d^{10} metallophilic attraction and the molecular properties precisely, one additional function was implemented for Ag (α_f = 0.22), Cu (α_f = 0.24), and P (α_d = 0.34).[2–4] The basis sets were taken as Ag(8s6p4d1f/3s3p2d1f), Cu(8s5p5d1f/3s3p2d1f), P(3s3p1d/2s2p1d), N(10s5p/3s2p), C(10s5p/3s2p), and H(4s/2s). Thus, 152 basis functions and 80 electrons for **2** and **3** and 218 basis functions and 124 electrons for **2**·$(MeCN)_2$ and **3**·$(MeCN)_2$ were included in the calculations.

Results and Discussion

Ground-State Structures

We used the MP2 method to fully optimize the ground-state structures of **2** and **3** and solvated species **2**·$(MeCN)_2$ and **3**·$(MeCN)_2$. Their structures are depicted in Figure 1. Under the C_i symmetry, these complexes have ^1A_g ground states. The main optimized geometry parameters are listed in Table 1 and Table 2, together with the data from X-ray crystal diffraction studies for $[M_2(dcpm)_2]\cdot(X)_2$ (M = Ag, X = $CF_3SO_3^-$; M = Cu, X = ClO_4^-).[28,29] For **2** and **3**, the d^{10} metal atoms take on a nearly linear two-coordinate geometry; the calculated P–M–P angles are 178.9° and 179.1°, comparable to the experimental values of 172.4° and 162.5°, respectively, as shown in Table 1. In the crystalline structure, the cation–anion interactions (M···O = 2.692 and 2.687 Å for the Ag and Cu complexes, respectively) result in a large difference between the calculated and experimental results.

Table 1. Optimized geometry parameters of $[Ag_2(dpm)_2]^{2+}$ (**2**) and $[Cu_2(dpm)_2]^{2+}$ (**3**) using the MP2 method for the ^1A_g ground state and the CIS method for the ^1A_u and ^3A_u excited states.

	2				**3**			
Parameters	^1A_g	Exp.[a]	^1A_u	^3A_u	^1A_g	Exp.[a]	^1A_u	^3A_u
Bond length [Å]								
M–M	3.160	2.960	2.981	3.056	3.061	2.731	2.667	2.704
M–P	2.498	2.405	2.827	2.840	2.230	2.229	2.566	2.543
P···P	3.112		3.116	3.125	3.099		3.125	3.113
Bond angle [°]								
P–M–P	178.9	172.4	177.3	178.6	179.1	162.5	169.8	170.8
P–M–M	89.5	91.8	91.4	90.7	90.5		95.1	94.6
Dihedral angle [°]								
P–M–M–P	180.0		180.0	180.0	180.0		180.0	180.0

[a] Experimental values of $[Ag_2(dcpm)_2]\cdot(CF_3SO_3)_2$ and $[Cu_2(dcpm)_2]\cdot(ClO_4)_2$ are from ref.[27] and ref.[28], respectively.

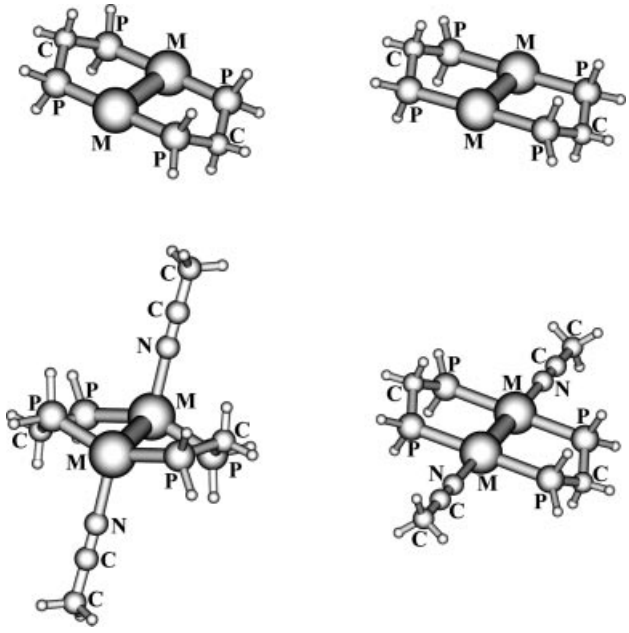

Figure 1. Ground- (left side) and excited- (right side) state structures for $[M_2(dpm)_2]^{2+}$ [M = Ag (**2**) and Cu (**3**)] and their weakly solvated species $[M_2(dpm)_2]^{2+}\cdot(MeCN)_2$.

The calculated 180.0° dihedral angles of P–M–M–P for **2** and **3** indicate that the M_2P_4 unit is coplanar. However, the interaction between the M(I) atom and acetonitrile in **2**·$(MeCN)_2$ and **3**·$(MeCN)_2$ results in M_2P_4 distortion from the original planarity, which is reflected by the calculated P–M–M–P dihedral angles of 151.3° and 138.4° (Table 2). The M–N distances are 2.380 and 1.976 Å for **2**·$(MeCN)_2$ and **3**·$(MeCN)_2$, respectively, which are very close to the experimental distances of 2.382 and 2.029 Å for $[Ag_2(dppa)_2(MeCN)_2]\cdot(PF_6)_2$ (dppa = $Ph_2PNHPPh_2$)[22] and $[Cu_2(dcpm)_2(MeCN)_2]\cdot(Y)_2$ (Y^- = ClO^- and BF_4^-)[29,30] and similar to the distances of 2.116 and 1.886 Å for $[M_2(form)_2]$ [M = Ag and Cu, form = (*p*-$CH_3C_6H_4$)NCHN(*p*-$CH_3C_6H_4$)].[55] In previous studies,[13] the calculated Au–N distance in **1**·$(MeCN)_2$ is 2.600 Å (Table S1 of the Supporting Information), which is much longer than the Au–N distance of 2.090 Å in $[Au_2(dpim)_2]\cdot(ClO_4)_2$ [dpim = 2-(diphenylphosphanyl)-1-methylimidazole].[56] Our calculated M–N distances for **1**–**3** in acetonitrile suggest that the M···N interactions are strong enough to form an M–N single bond for the Ag and Cu complexes, but very weak in the Au complex. The M–N bonding energies in (**1**–**3**)·$(MeCN)_2$ were estimated by using the Counterpoise method at the MP2 level. They are approximately 18.9, 27.0, and 36.5 kcal/mol, respectively. The present studies substantiate the previous conclusion that the Au^I atom favors a linear two-coordinate arrangement, while the Ag^I and Cu^I atoms have the formal three coordination.[57]

Table 2. Optimized geometry parameters of $[Ag_2(dpm)_2]^{2+}\cdot(MeCN)_2$ [**2**·$(MeCN)_2$] and $[Cu_2(dpm)_2]^{2+}\cdot(MeCN)_2$ [**3**·$(MeCN)_2$] using the MP2 method for the ^1A_g ground state and the CIS method for the ^1A_u and ^3A_u excited states.

	2·$(MeCN)_2$			**3**·$(MeCN)_2$		
Parameters	^1A_g	^1A_u	^3A_u	^1A_g	^1A_u	^3A_u
Bond length [Å]						
M–M	3.069	2.986	3.046	2.875	2.920	3.003
M–P	2.517	2.917	2.838	2.299	2.768	2.646
M–N	2.380	2.401	2.441	1.976	2.102	2.149
P···P	3.073	3.063	3.086	3.034	3.042	3.061
Bond angle [°]						
P–M–P	150.9	178.4	179.2	138.1	177.4	178.7
P–M–M	92.6	90.7	90.4	93.7	91.3	90.6
N–M–M	109.5	179.8	179.8	113.9	179.8	180.0
Dihedral angle [°]						
P–M–M–P	151.3	179.5	179.7	138.4	179.7	179.9

The M(I)–M(I) separations that were calculated are 3.033, 3.160, and 3.061 Å for **1**–**3** in the ground states, which correspond to the experimental data of 2.939, 2.960, and 2.731 Å, respectively.[26,28,29] There is a large difference, especially for the Ag and Cu complexes. The following two reasons may be responsible for this. First, the choice of basis sets may cause such a difference. Hence, the SDD basis set, which is larger than the LanL2DZ basis set, was used to optimize **1**–**3** in order to judge the basis-set effect. The calculated results show that the Ag–Ag distance is shortened by about 0.1 Å but the Au–Au and Cu–Cu distances are nearly unchanged upon increasing the basis sets as shown in Table S2 of the Supporting Information. Second, in our calculations we used the model complex $[M_2(dpm)_2]^{2+}$ to replace the real complex $[M_2(P–P)_2]^{2+}$ (P–P = dmpm, dppm, and dcpm). This substituent approximation may affect the geometry parameters of the complexes. In Table S2,

we list the optimized geometry parameters of $[M_2(dmpm)_2]^{2+}$ (M = Au, Ag, and Cu) and the data for $[M_2(P–P)_2](X)_2$ (M = Au, Ag, and Cu; P–P = dmpm, dppm, and dcpm; X = counteranion) that were determined from experiments.[22,26,28,29,40–45] One can see that the calculated results have now improved. The M–M distances of $[M_2(dmpm)_2]^{2+}$ (M = Au, Ag, and Cu) are 2.985, 3.021 and 2.818 Å, respectively and approach the experimental values. Table S2 of the Supporting Information indicates that although the use of the larger basis sets (SDD) and heavy substituent on the phosphorous atoms (e.g. dmpm ligand) in the calculations presents results that are closer to the experimental values, the calculated results for $[M_2(dpm)_2]^{2+}$ with the LanL2DZ basis sets can also describe the essential characteristics of real complexes.

The natural bond orbital (NBO) analysis[58–60] using the MP2 density shows that the M atoms of **1**–**3** have net electronic charges of +0.31, +0.56, and +0.56, respectively, while electronic charges residing on the P atoms are +0.39, +0.28, and 0.27. This indicates that the electrons of the P atoms transfer to the original $(n + 1)$s and $(n + 1)$p empty orbitals of M(I). Consequently, the closed-shell electronic configurations, $nd^{10}(n + 1)s^0$, are no longer kept in **1**–**3** but become $5d^{9.76}6s^{0.87}6p^{0.03}4f^{0.03}$ (Au), $4d^{9.89}5s^{0.52}5p^{0.02}4f^{0.01}$ (Ag), and $3d^{9.86}4s^{0.56}4p^{0.02}4f^{0.01}$ (Cu) instead. Because the relativistic effects are stronger on Au than on Ag and Cu,[61] there is more 5d→6(s, p) population transfer for the Au atom. Such a destruction of metal closed-shell structures may be one of the predominant driving forces in causing metallophilic attraction.

Absorption Spectra

According to the vertical electron-transition mechanism in the absorption process, the optimized ground-state structures of (**1**–**3**)·$(MeCN)_2$ were kept, while TD-DFT (B3LYP) calculations were performed in order to calculate the excited states related to the absorption. With respect to the ^1A_g ground state under the C_i point group, the ^1A_g→^1A_u transition is spin-dipole-allowed. We obtained low-lying dipole-allowed transitions of (**1**–**3**)·$(MeCN)_2$ that represent the possible absorptions of **1**–**3** in acetonitrile. Transition energies (eV/nm) of these absorptions are presented in Table 3, together with the corresponding oscillator strengths and experimental values available.[8,25,28,29,31,32,39] In order to conveniently assign the calculated electronic absorptions, the electron density diagrams of the frontier molecular oribitals involved in the transitions are displayed in Figure 2.

For **1**·$(MeCN)_2$, we obtained three low-lying absorptions from the TD-DFT calculations. In Figure 2, one can see that the orbitals involved in the transitions are mainly Au in character. The analyses of the wave functions of **1**·$(MeCN)_2$ suggest that the $29a_u$ (HOMO–3), $30a_u$ (HOMO–2), $31a_u$ (HOMO), and $32a_g$ (LUMO) orbitals mainly have σ(Au–P), $\sigma^*(d_{y^2-z^2})$, $\sigma^*(s, d_{z^2})$, and $\sigma(sp_z)$ character, respectively (the Au_2P_4 unit lies in the *xz* plane and the *z* axis goes through the two Au atoms).

The lowest-energy absorption of **1** in acetonitrile was calculated at 291 nm, which results from the $31a_u$→$32a_g$ (HOMO→LUMO) configuration with the largest CI coefficient of 0.673 in the wave functions (Table 3). We attributed this absorption to a metal-centered $\sigma^*(s, d_{z^2})$→$\sigma(sp_z)$ transition. It has been found that $[Au_2(P–P)_2]^{2+}$ (P–P = dmpm, dppm, and dcpm)[8,25,31,32,39] display intense absorption bands at 269, 292, and 278 nm in acetonitrile, respectively. These absorptions correspond to the calculated 291-nm absorption and also arise from a $\sigma^*(s, d_{z^2})$→$\sigma(sp_z)$ transition. The B^1A_u excited state of **1**·$(MeCN)_2$ gives the absorption at 237 nm, which corresponds to the experimental absorption at 239–267 nm (in Table 3).[8,25,31,32,39] The absorption also has the nature of a MC transition, a $\sigma^*(d_{y^2-z^2})$→$\sigma(sp_z)$ transition. There is much contribution from the phosphane ligands for the X^1A_g→C^1A_u transition, which is intuitively reflected in Figure 2. We assigned the 224-nm absorption to a σ(Au–P)→$\sigma(sp_z)$ transition.

With respect to analogous Ag and Cu complexes, we obtained three and four low-lying electronic transitions in ace-

Table 3. Calculated absorptions of $[Au_2(dpm)_2]^{2+}$·$(MeCN)_2$, $[Ag_2(dpm)_2]^{2+}$·$(MeCN)_2$, and $[Cu_2(dpm)_2]^{2+}$·$(MeCN)_2$ at the TD-DFT (B3LYP) level.

	States	Conf.	|CI coeff.| > 0.2	Trans. ener.		*f*	Exp. [nm][a]		
				[nm]	[eV]		dcpm	dmpm	dppm
Au	A^1A_u	$31a_u$→$32a_g$	0.67310	291	4.26	0.162	278	269	292
	B^1A_u	$30a_u$→$32a_g$	0.68089	237	5.23	0.050	243	239	267
	C^1A_u	$29a_u$→$32a_g$	0.68087	224	5.53	0.022		213	
Ag	A^1A_u	$31a_u$→$32a_g$	0.68321	256	4.84	0.132	261		
	B^1A_u	$30a_u$→$32a_g$	0.68629	238	5.22	0.070			
	C^1A_u	$31a_u$→$33a_g$	0.43752	201	6.18	0.003			
		$29a_u$→$32a_g$	0.42265						
		$31a_g$→$32a_u$	0.25181						
Cu	A^1A_u	$31a_u$→$32a_g$	0.53146	283	4.39	0.036	319		
		$30a_u$→$32a_g$	–0.43078						
	B^1A_u	$29a_u$→$32a_g$	0.68166	246	5.04	0.071	269		
	C^1A_u	$28a_u$→$32a_g$	0.67986	231	5.38	0.011			
	D^1A_u	$27a_u$→$32a_g$	0.66148	219	5.66	0.009			

[a] The absorptions in acetonitrile of $[M_2(dcpm)_2]^{2+}$ (M = Au, Ag, and Cu) are from ref.[24], ref.[27] and ref.[28], respectively. The results of $[Au_2(dmpm)_2]^{2+}$ are from ref.[8] and those of $[Au_2(dppm)_2]^{2+}$ from ref.[30,31,38]

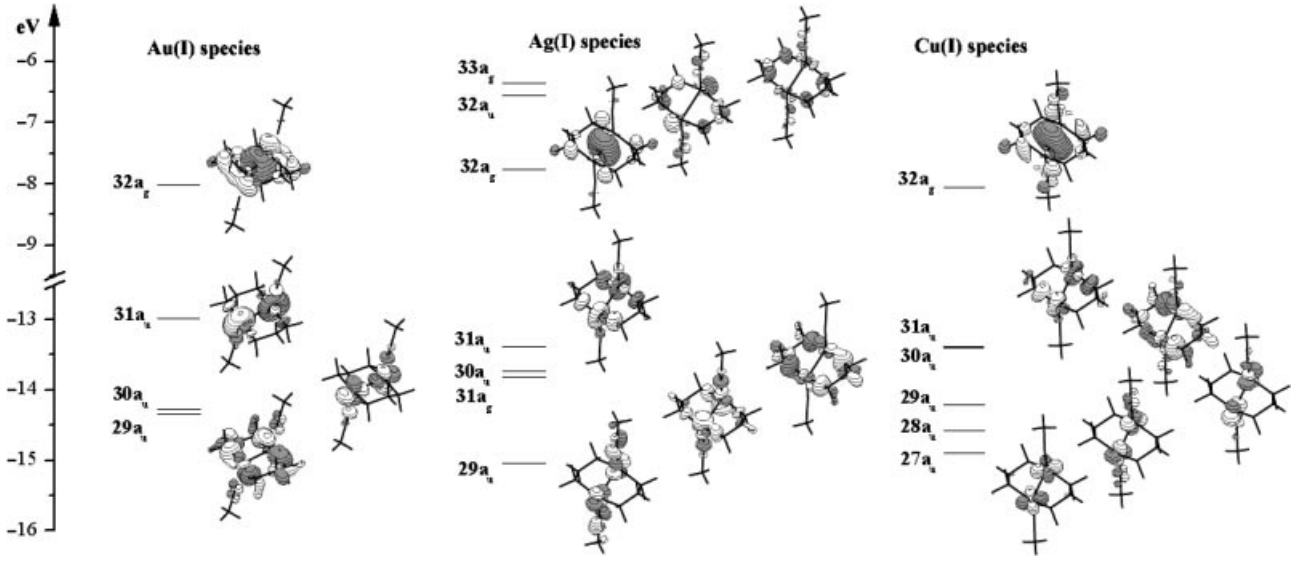

Figure 2. Frontier molecular diagrams of $[M_2(dpm)_2]^{2+}\cdot(MeCN)_2$ (M = Au, Ag, and Cu) in the TD-DFT (B3LYP) calculations.

tonitrile, respectively. By combining the information from Table 3 and Figure 2, one can see that **2** and **3** have relatively more complicated transitions than **1**. The calculated lowest-energy absorption of 256 nm for **2** in acetonitrile was assigned to a $\sigma^*(s, d_{z^2})\rightarrow\sigma(sp_z)$ transition, with a maximum oscillator strength of 0.132; we relate this to the 261-nm absorption band of $[Ag_2(dcpm)_2]^{2+}$ recorded in acetonitrile.[28] The lowest-energy absorption of 283 nm for **3** in acetonitrile is not a pure metal-centered $\sigma^*(s, d_{z^2})\rightarrow\sigma(sp_z)$ transition, which is different from those of **1** and **2**. The absorption (Table 3) results from the $31a_u\rightarrow32a_g$ (HOMO→LUMO) and $30a_u\rightarrow32a_g$ (HOMO–1→LUMO) configurations and is attributed to the mixture of $\sigma^*(s, d_{z^2})\rightarrow\sigma(sp_z)$ and $\sigma(Cu–P)\rightarrow\sigma(sp_z)$ transitions. Our calculated absorptions agree well with the experimental observations and provide more detailed information about the transition properties of the absorptions.

Such analyses show that relativistic effects play a significant role in the electronic transitions of **1**–**3** in acetonitrile, especially for the lowest-energy HOMO→LUMO transitions. As far as **1**–**3** are concerned, relativistic effects destabilize the $\sigma^*[nd_{z^2}(M_2)]$ orbital but stabilize the $\sigma[(n + 1)sp_z(M_2)]$, which result in the net effect of a decrease in the HOMO–LUMO energy gap. Because the later-row transition metals have stronger relativistic effects, **1** has a smaller HOMO–LUMO gap (Figure 2) and lower-energy HOMO→LUMO absorption than **2** and **3** (Table 3). Since the relativistic effects of Ag are larger than those of Cu, **2** should have a lower HOMO→LUMO absorption in acetonitrile. However, this is not the case in the present calculations (Table 3). We think that the M–M interactions are also one of the more important factors that affect the transition energies for **2** and **3**. Table 2 shows that the M–M distance of 2.875 Å for **3** is much shorter than that of 3.069 Å for **2**, which greatly facilitates the lower-energy transition for the Cu complex. It could be said[1] that among the coinage metals (Au, Ag, and Cu), only silver is "normal". As already mentioned, gold is anomalous because of its large relativistic effects. As the underlying nodeless d shell of copper is more compact than that of silver or gold, copper is often seen to behave differently. This suggestion has been, to some extent, reflected in such studies on the electronic absorptions of **1**–**3**. Additionally, it is worth noting that the spin-orbit interactions are an important influence on the transition moments, even if they are perhaps quenched in the molecular field.

In addition, we also calculated the absorptions of **1**–**3** in the acetonitrile solution using the CIS method. Their lowest-energy absorptions mainly feature the HOMO→LUMO transitions and the $\sigma^*(s, d_{z^2})\rightarrow\sigma(sp_z)$ characters, as do those from the TD-DFT calculations. However, the transition energies of 5.60, 6.66, and 6.68 eV for **1**–**3**, respectively, from the CIS calculations were severely overestimated relative to the experimental values. The TD-DFT calculations yield a better estimation of transition energies of absorptions than the CIS method.

Excited-State Structures

To describe the luminescent properties of **2** and **3**, the CIS method was used to optimize the excited-state structures, both in the gas phase and in acetonitrile. Their structures are shown in Figure 1 and the main optimized geometry parameters are listed in Table 1 and Table 2.

With respect to the $^1A_u/^3A_u$ excited states of **2** and **3**, the optimized structures show significant changes compared with those of their corresponding ^1A_g ground states as can be seen in Table 1. The M(I)–M(I) distances are shortened from 3.160 and 3.061 Å to 2.981/3.056 and 2.667/2.704 Å for **2** and **3**, respectively. The bonding interactions between the two M(I) atoms in the $^1A_u/^3A_u$ excited states weaken the P→M dative bonds.

In solution, the acetonitrile molecules coordinate to the metal atoms of **2** and **3** with N–M–M angles of 109.5° and

113.9° in the ^1A_g ground states, respectively; in the $^1A_u/^3A_u$ excited states, the N–M–M angles are close to 180° (Table 2). The M–N interactions in **2**·$(MeCN)_2$ and **3**·$(MeCN)_2$ are slightly weaker in the $^1A_u/^3A_u$ excited states than in the ground states, thus elongating by ca. 0.02/0.06 and 0.03/0.07 Å, respectively. However, the interaction between the Au^I and N atoms in acetonitrile is greatly enhanced in the excited states since the Au–N distances of the $^1A_u/^3A_u$ excited states are about 0.17/0.22 Å shorter than that of the ^1A_g ground state (Table S1 of Supporting Information). Our previous studies on **1** showed that the N→Au coordination in acetonitrile results in about a 200-nm red-shift of the emission wavelength in the ^3A_u excited state.[13] Thus, we conjecture that the influence of acetonitrile on emissions of **2** and **3** is not as significant as on **1**.

To certify the validity of the CIS-optimized geometries, we used the unrestricted MP2 method (UMP2) to optimize the lowest-energy triplet excited states of **1**–**3**. The main optimized geometry parameters of the ^3A_u excited states are given in Table 4. The wave functions of the excited states demonstrate that the HOMOs are the σ bonding orbitals, mainly contributed to by the metal $(n + 1)(sp_z)$ atomic orbitals, and the LUMOs possess $\sigma^*(nd_{z^2})$ character. The ^3A_u excited state from the UMP2 calculations has orbital character that is very similar to that of the ^3A_u excited state from the CIS calculations for each complex. Thus, the $^3[\sigma^*(d)\sigma(sp)]$ states from the UMP2 calculations correspond to those from the CIS calculations. In comparison with those optimized by the CIS method, the geometry parameters of the ^3A_u excited states from the UMP2 method are more unrelaxed (Table 1 and Table 4). This is because the latter includes more electron correlation effects.[2–4] Despite some differences between the UMP2 and CIS methods in optimized geometry parameters for **1**–**3**, the two methods can reasonably predict the excited-state properties of the complexes.

Table 4. Optimized geometry parameters of the lowest-energy ^3A_u triplet excited states by the UMP2 method for $[Au_2(dpm)_2]^{2+}$ (**1**), $[Ag_2(dpm)_2]^{2+}$ (**2**), and $[Cu_2(dpm)_2]^{2+}$ (**3**).

Parameters	**1**[a]	**2**	**3**
Bond length [Å]			
M–M	2.678	2.709	2.408
M–P	2.404	2.545	2.307
P···P	3.109	3.125	3.385
Bond angle [°]			
P–M–P	169.7	170.6	155.5
P–M–M	95.1	94.7	102.2
Dihedral angle [°]			
P–M–M–P	180.0	179.3	179.3

[a]. The results of the ^3A_u triplet excited state of $[Au_2(dpm)_2]^{2+}$ (**1**) are from ref.[13]

We have performed the frequency calculations on **1**–**3** at the MP2 level for the ground and triplet excited states. No imaginary frequencies available indicate that these ground- and excited structures are minimum points. The calculated M–M stretching frequencies (Table 5) are ca. 89, 69, and 69 cm^{-1} for **1**–**3** in the ground states, which are comparable to the experimental data of 88, 80, and 104 cm^{-1} for $[Au_2(dcpm)_2]\cdot(ClO_4)_2$,[27] $[Ag_2(dcpm)_2]\cdot(CF_3SO_3)_2$,[28] and $[Cu_2(dcpm)_2]\cdot(ClO_4)_2$,[29] respectively. Keeping the experimental M–M distances from the MP2 calculations, we optimized the structures of **1**–**3** and present the calculated M–M frequencies in Table 5. The M–M stretching frequencies provide evidence for weak metallophilic attraction between the two d^{10} metal atoms in the ground states.

Relative to those in the ground states, the M–M stretching frequencies greatly increase in the ^3A_u excited states. The 144, 142, and 170 cm^{-1} M–M stretching frequencies of **1**–**3** correspond to 175, 180, and 150 cm^{-1} frequencies estimated by Raman Resonance spectroscopy, respectively.[27–29] Such MP2 calculations suggest that the M–M interaction is weak in the ground state (mean M–M dis-

Table 5. Calculated Au–Au stretching frequencies for the ground states and lowest-energy triplet excited states of $[Au_2(dpm)_2]^{2+}$ (**1**), $[Ag_2(dpm)_2]^{2+}$ (**2**), $[Cu_2(dpm)_2]^{2+}$ (**3**), and related dinuclear Au^I complexes at the MP2 level, together with the data from the Raman Resonance spectra.[a]

	Ground state			Triplet excited state		
	M–M [Å]	Freq. [cm^{-1}]		M–M [Å]	Freq. [cm^{-1}]	
		Calcd.	Exp.		Calcd.	Exp.
1	3.033 (2.939)[b]	89 (104)[c]	88	2.678	144	175
2	3.160 (2.960)[b]	69 (94)[c]	80	2.709	142	180
3	3.061 (2.731)[b]	69 (89)[c]	104	2.408	170	150
4[d]	2.913	110		2.787	135	
5[d]	2.945	96		2.786	119	
6[d]	3.011	93		2.778	126	
7[d]	2.989	96		2.620	164	
8[d]	2.979	96		2.619	165	
9[d]	2.972	97		2.572	189	
10[d]	2.944	101		2.583	179	

[a] The M–M frequencies of Raman Resonance spectra are from ref.[26–28]. [b] The M–M distances in parentheses were determined from X-ray crystal diffraction studies for $[Au_2(dcpm)_2]\cdot(ClO_4)_2$,[25] $[Ag_2(dcpm)_2]\cdot(CF_3SO_3)_2$,[27] and $[Cu_2(dcpm)_2]\cdot(ClO_4)_2$[28]. [c] The M–M stretching frequencies in parentheses were obtained on the basis of the optimized geometries of **1**, **2**, and **3** with the fixed experimental M–M distances. [d] Complexes **4**–**10** are $[Au_2(PH_2CH_2PH_2)(i\text{-}mnt)]$, $[Au_2(PH_3)_2(i\text{-}mnt)]$, $[Au_2(PH_2CH_2PH_2)(SCH_2S)]$, $[Au_2(PH_2CH_2PH_2)(SHCH_2SH)]^{2+}$, *trans*-$[Au_2(PH_2CH_2SH)_2]^{2+}$, *cis*-$[Au_2(PH_2CH_2SH)_2]^{2+}$, and $[Au_2(SHCH_2SH)_2]^{2+}$ (i-mnt = i-malononitriledithiolate), respectively. Their Au–Au distances and stretching frequencies are from ref.[13] and ref.[16], respectively.

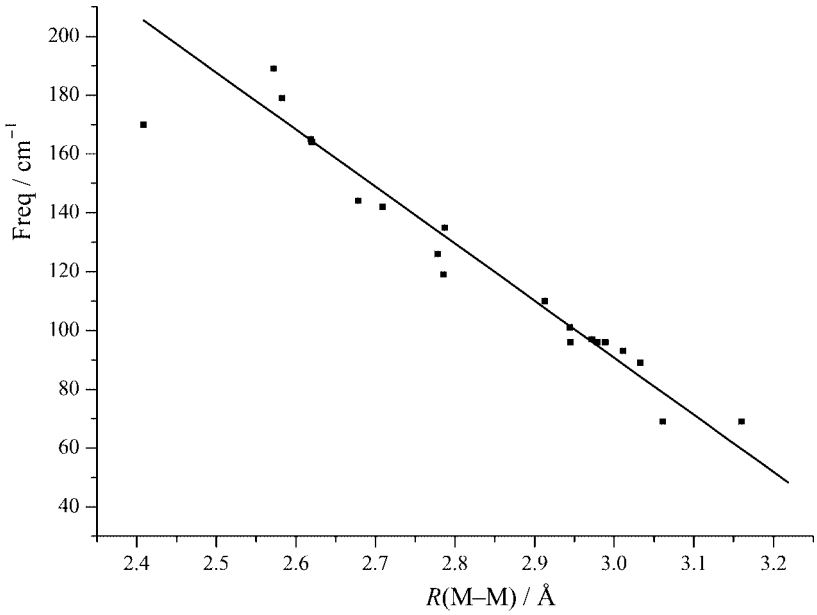

Figure 3. Plot of M–M distances versus stretching frequencies in the ground and lowest-energy triplet excited states for a series of dinuclear d^{10} complexes, **1**–**10**, from the MP2 and UMP2 calculations, respectively.

tance: 3.10 Å, and M–M stretching frequency: 80 cm^{-1}), but is strongly enhanced in the triplet excited state (mean M–M distance: 2.60 Å, and M–M stretching frequency: 150 cm^{-1}).

In Table 5, we summarize the calculated M–M distances and stretching frequencies in the ground and lowest-energy triplet excited states for a series of dinuclear d^{10} complexes, **1**–**10**, from MP2 and UMP2 calculations, respectively.[13,16] The plot of the M–M distances versus stretching frequencies in Figure 3 intuitively illustrates that the M–M distances are linearly correlated with the M–M stretching frequencies for the dinuclear d^{10} complexes.

Emission Spectra

It has been found that the CIS excited-state geometries are more accurate than the CIS transition energies as indicated in the literature.[62,63] The large deviations in the excitation energies are caused by an unbalanced description of the ground- and excited states. TD-DFT calculations, based on linear-response theory, have recently been reformulated to yield better transition energies than the CIS method.[63–66] Since the CIS method can present the accurate excited-state geometry and potential-energy surface, and the TD-DFT calculations can reasonably predict the

Table 6. Calculated emissions of $[Au_2(dpm)_2]^{2+}$ (**1**), $[Ag_2(dpm)_2]^{2+}$ (**2**) and $[Cu_2(dpm)_2]^{2+}$ (**3**) in the gas phase, solid state and acetonitrile solution at the CIS and TD-DFT (B3LYP) levels.

			CIS		TD-DFT		Exp.[a]		
			λ [nm/eV]	*f*	λ [nm/eV]	*f*	dcpm	dmpm	dppm
1	Gas phase	^1A_u	247/5.03	0.303	318/3.89	0.161			
		^3A_u	301/4.12		381/3.25				
	Solid state[b]	^3A_u	304/4.08		402/3.08		368		
	Solution	^1A_u	339/3.66	0.188	484/2.56	0.116			
		^3A_u	507/2.44		818/1.51		490–530	555	565–593
2	Gas phase	^1A_u	216/5.75	0.127	302/4.11	0.088			
		^3A_u	259/4.78		356/3.49				
	Solid state[b]	^3A_u	263/4.71		366/3.39		417		
	Solution	^1A_u	238/5.19	0.130	366/3.39	0.093			
		^3A_u	277/4.48		424/2.93				
3	Gas phase	^1A_u	214/5.78	0.187	328/3.78	0.094			
		^3A_u	252/4.93		397/3.13				
	Solid state[b]	^3A_u	258/4.81		424/2.92		475		
	Solution	^1A_u	249/4.97	0.122	435/2.85	0.084			
		^3A_u	281/4.41		514/2.41		480		

[a] The emissions of $[M_2(dcpm)_2]^{2+}$ (M = Au, Ag, and Cu) in acetonitrile are from ref.[24,25], ref.[27] and ref.[28,29], respectively. The results of $[Au_2(dmpm)_2]^{2+}$ are from ref.[8] and those of $[Au_2(dppm)_2]^{2+}$ from ref.[30,31,38]. [b] The results from $[M_2(dpm)_2]\cdot(ClO)_2$ (M = Au, Ag, and Cu) with fixed experimental M···O distances of 3.362, 2.692, and 2.687 Å, respectively.

transition energies, the combination of the benefits of the two methods is a practical approach to describe the excited-state properties of molecules.

In this paper, we have used the CIS method to optimize the lowest-energy singlet and triplet excited states for **2** and **3** and their solvated species. On the basis of these optimized structures, the TD-DFT (B3LYP) method was performed to calculate the emission spectra of **2** and **3** in the gas phase and in solution. The calculated emissions are listed in Table 6, together with the experimental values for $[M_2(dcpm)_2]\cdot(X)_2$ (M = Ag, X = $CF_3SO_3^-$; M = Cu, X = ClO_4^-).[28–30]

From the TD-DFT calculations, the $^1A_u/^3A_u$ excited states of **2** and **3** give rise to the 302/356 and 328/397-nm emissions in the gas phase, and 366/424 and 435/514-nm emissions in acetonitrile, respectively. According to the analyses of the wave functions of these excited states, we attribute the emissions to the metal-centered σ(s, p_z)→σ*($d_{x^2-z^2}$, d_{y^2}) transitions, as is the case for those of **1** in previous studies.[13] The detailed information on the electronic structures of the ^3A_u excited states for **1**–**3** are presented in Table S3 of the Supporting Information, contributing to our understanding of such MC transitions. Compared with those in the gas phase, the calculated emissions in acetonitrile are red shifted by about 64/68 and 107/117 nm for the $^1A_u/^3A_u$ excited states of **2** and **3**, respectively. The interactions between cation and solvent molecules result in a large red shift. Since the lowest-energy emissions of **1**–**3** arise from the metal-centered σ(s, p_z)→σ*($d_{x^2-z^2}$, d_{y^2}) transitions, either in the gas phase or in solution, we think that the dinuclear d^{10} complexes with bridging phosphane ligands have the intrinsic ^{1,3}[σ*(d)σ(s/p)] excited states.

In the crystalline phase of $[Ag_2(dcpm)_2]\cdot(CF_3SO_3)_2$[28] and $[Cu_2(dcpm)_2]\cdot(ClO_4)_2$,[29] very close cation-anion contacts were determined by X-ray crystal diffraction [2.692 and 2.687 Å (M···O), respectively]. The presence of anions near the $[M_2(dcpm)_2]^{2+}$ cations affects the solid-state emission. In previous studies of **1**,[12] the less bulky ClO^- anion was used to replace the original ClO_4^- anion in the $[Au_2(dcpm)_2]\cdot(ClO_4)_2$ crystalline phase, i.e. **1**·$(ClO)_2$ was applied to simulate the solid-state behaviors of the Au complex. Similar models, **2**·$(ClO)_2$ and **3**·$(ClO)_2$, were used in the calculations in order to represent the real complexes, $[Ag_2(dcpm)_2]\cdot(CF_3SO_3)_2$ and $[Cu_2(dcpm)_2]\cdot(ClO_4)_2$, respectively. When the *R*(M–OCl) distance changes from 5.5 to 2.5 Å, the corresponding phosphorescent emission varies in the ranges 382–535, 398–440, and 356–370 nm for the Au, Ag and Cu complexes, respectively. Figure 4 clearly reflects the correlation between the emission wavelength and *R*(M–OCl) for **1**–**3**·$(ClO)_2$. The emission of **1**·$(ClO)_2$ is very sensitive to the *R*(M–OCl) distance, especially when *R*(M–OCl) < 3.5 Å, while those of **2**·$(ClO)_2$ and **3**·$(ClO)_2$ are relatively insensitive. When *R*(M–OCl) > 4.0 Å, the anion slightly affects the emissions of the complexes. Keeping the experimental M···O distances 3.362, 2.692, and 2.687 Å in the calculations on $[M_2(dpm)_2]\cdot(ClO)_2$ (M = Au, Ag, and Cu), respectively, we obtained the emissions of **1**–**3** in the solid state. The calculated phosphorescent emissions are 402, 366, and 424 nm, which are comparable to the experimental emissions of 368, 417, and 475 nm in the solid state, respectively.[28,29]

From Table 6, one can see that the CIS method overestimates the emission energies by ca. 2 eV with respect to the experimental values for the Ag and Cu complexes, while those predicted by TD-DFT are closer to the experimental values. For **3**, the phosphorescent emissions were calculated at 4.81 eV (258 nm) and 4.41 eV (281 nm) in the solid state and acetonitrile, respectively, while the experimental values were severely overestimated [2.61 eV (475 nm) and 2.58 eV (480 nm)] for $[Cu_2(dcpm)_2]\cdot(ClO_4)_2$.[29,30] TD-DFT calculations were carried out at the CIS-optimized excited-state

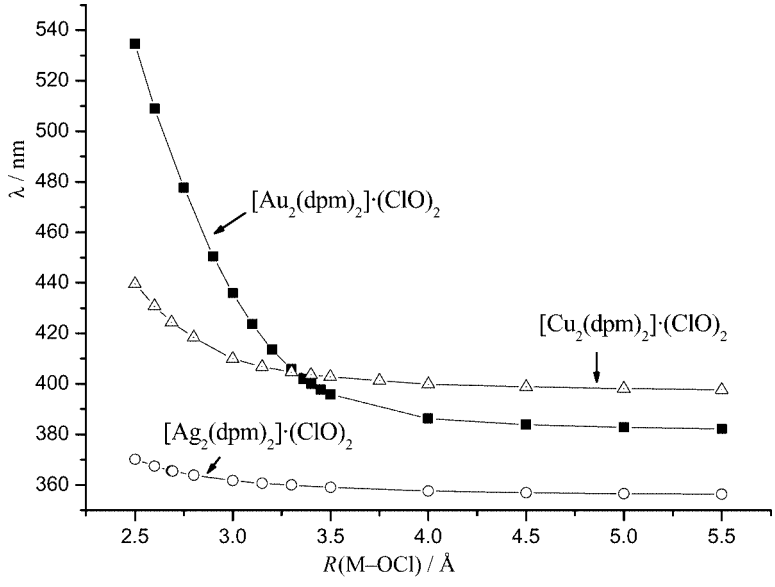

Figure 4. Plot of emission wavelength versus *R*(M–OCl) (distance between M atom and ClO^- anion) for $[M_2(dpm)_2]^{2+}\cdot(ClO)_2$ (M = Au, Ag, and Cu) in the TD-DFT (B3LYP) calculations.

structure to obtain more accurate estimates of the emission energies. With TD-DFT, the phosphorescent emission energies were predicted to be 2.92 eV (424 nm) and 2.41 eV (514 nm) in the solid state and in acetonitrile, respectively, which are much closer to the experimental observations. However, with respect to the Au complex, the CIS and TD-DFT calculations over- and underestimated the emission energies, respectively, relative to the available experimental data.[8,25,26,31,32,39]

Conclusions

In the paper, we used theoretical methods to study the electronic structures and spectroscopic properties of **2** and **3** and their solvated species. Taking previous studies into account on **1**,[13] we have come to the following conclusions.

For the dinuclear d^{10} complexes of **1**–**3**, the calculated M–M distances (3.03–3.16 Å) and their corresponding M–M stretching frequencies (69–89 cm^{-1}) at the MP2 level indicate the presence of metallophilic attraction in the ground states. This is also supported by the NBO analysis on the electronic configurations of the metal atoms. In acetonitrile, the N→M coordination is strong enough to form a σ single bond in the Ag and Cu species, but is very weak in the Au analog. This agrees with the usual coordinated geometries of the Au, Ag, and Cu atoms.

In the excited states of **1**–**3**, the M–M interactions are strengthened, resulting from the promotion of electrons from the σ*(d) antibonding orbital to the σ(s/p) bonding orbital upon excitation. These complexes give rise to the metal-centered $\sigma(s, p_z)\rightarrow\sigma^*(d_{x^2-z^2}, d_{y^2})$ emissions, both in the gas phase and in solution, revealing that the dinuclear d^{10} complexes with bridging phosphane ligands have the intrinsic $^{1,3}[\sigma^*(d)\sigma(s/p)]$ excited states. The comparison between the gas-phase and solution emissions for **1**–**3** shows that the N→M coordination results in a large red shift of the emission wavelength.

Taking previous studies into account, we found that the M–M distances are linearly correlated with the M–M stretching frequencies for the dinuclear d^{10} complexes in the ground and lowest-energy triplet excited states.

In comparison with experimental values, the CIS calculations severely overestimate the transition energies of the Ag and Cu complexes, but the TD-DFT calculations reasonably predict their transition energies. However, with respect to the Au analog, the CIS and TD-DFT methods over- and under-estimate the transition energies, respectively.

Supporting Information (see footnote on the first page of this article): Table of optimized geometry parameters of $[Au_2(dpm)_2]^{2+}$ (**1**) and **1**·$(MeCN)_2$ in the ground and excited states. Table of optimized geometry parameters of $[M_2(dmpm)_2]^{2+}$ (M = Au, Ag and Cu) in the MP2 calculations. Table of compositions of HOMO and LUMO for the ^3A_u excited states of **1**–**3** and **1**–**3**·$(MeCN)_2$ in the TD-DFT calculations.

Acknowledgments

This work was supported by the Natural Science Foundation of China (20301006, 20173021).

[1] P. Pyykkö, *Chem. Rev.* **1997**, *97*, 597–636.
[2] P. Pyykkö, *Angew. Chem. Int. Ed.* **2004**, *43*, 4412–4456.
[3] P. Pyykkö, N. Runeberg, F. Mendizabal, *Chem. Eur. J.* **1997**, *3*, 1451–1457.
[4] P. Pyykkö, F. Mendizabal, *Inorg. Chem.* **1998**, *37*, 3018–3025.
[5] É. Fournier, A. Dechken, P. D. Harvey, *Eur. J. Inorg. Chem.* **2004**, 4420–4429.
[6] M. A. Rawashdeh-Omary, M. A. Omary, H. H. Patterson, J. P. Fackler Jr., *J. Am. Chem. Soc.* **2001**, *123*, 11237–11247.
[7] M. Bardají, P. G. Jones, A. Laguna, M. D. Villacampa, N. Villaverde, *Dalton Trans.* **2003**, 4529–4536.
[8] V. W.-W. Yam, T.-F. Lai, C.-M. Che, *J. Chem. Soc., Dalton Trans.* **1990**, 3747–3752.
[9] A. A. Mohamed, I. Kani, A. O. Ramirez, J. P. Fackler Jr., *Inorg. Chem.* **2004**, *43*, 3833–3839.
[10] K. H. Leung, D. L. Phillips, Z. Mao, C.-M. Che, V. M. Miskowski, C.-K. Chan, *Inorg. Chem.* **2002**, *41*, 2054–2059.
[11] S. D. Hanna, J. I. Zink, *Inorg. Chem.* **1996**, *35*, 297–302.
[12] H.-X. Zhang, C.-M. Che, *Chem. Eur. J.* **2001**, *7*, 4887–4893.
[13] Q.-J. Pan, H.-X. Zhang, *J. Phys. Chem. A* **2004**, *108*, 3650–3661.
[14] Q.-J. Pan, H.-X. Zhang, *J. Chem. Phys.* **2003**, *119*, 4346–4352.
[15] Q.-J. Pan, H.-X. Zhang, *Chem. Phys. Lett.* **2004**, *394*, 155–160.
[16] Q.-J. Pan, H.-X. Zhang, *Organometallics* **2004**, *23*, 5198–5209.
[17] Q.-J. Pan, H.-X. Zhang, *Eur. J. Inorg. Chem.* **2003**, 4202–4210.
[18] H. Schmidbaur, *Chem. Soc. Rev.* **1995**, *24*, 391–400.
[19] E. J. Fernández, J. M. López-de-Luzuraga, M. Monge, M. A. Rodríguez, O. Crespo, M. C. Gimeno, A. Laguna, P. G. Jones, *Inorg. Chem.* **1998**, *37*, 6002–6006.
[20] P. Schwerdtfeger, A. E. Bruce, M. R. M. Bruce, *J. Am. Chem. Soc.* **1998**, *120*, 6587–6597.
[21] L. Magnko, M. Schweizer, G. Rauhut, M. Schütz, H. Stoll, H.-J. Werner, *Phys. Chem. Chem. Phys.* **2002**, *4*, 1006–1013.
[22] H. Liu, M. J. Calhorda, M. G. B. Drew, V. Félix, J. Novosad, L. F. Veiros, F. F. De Biani, P. Zanello, *J. Chem. Soc., Dalton Trans.* **2002**, 4365–4374.
[23] H. L. Hermann, G. Boche, P. Schwerdtfeger, *Chem. Eur. J.* **2001**, *7*, 5333–5342.
[24] P. D. Harvey, M. Drouin, T. Zhang, *Inorg. Chem.* **1997**, *36*, 4998–5005.
[25] W.-F. Fu, K.-C. Chan, V. M. Miskowski, C.-M. Che, *Angew. Chem. Int. Ed.* **1999**, *38*, 2783–2785.
[26] W.-F. Fu, K.-C. Chan, K.-K. Cheung, C.-M. Che, *Chem. Eur. J.* **2001**, *7*, 4656–4664.
[27] K. H. Leung, D. L. Phillips, M.-C. Tse, C.-M. Che, V. M. Miskowski, *J. Am. Chem. Soc.* **1999**, *121*, 4799–4803.
[28] C.-M. Che, M.-C. Tse, M. C. W. Chan, K.-K. Cheung, D. L. Phillips, K.-H. Leung, *J. Am. Chem. Soc.* **2000**, *122*, 2464–2468.
[29] C.-M. Che, Z. Mao, V. M. Miskowski, M.-C. Tse, C.-K. Chan, K.-K. Cheung, D. L. Phillips, K.-H. Leung, *Angew. Chem. Int. Ed.* **2000**, *39*, 4084–4088.
[30] W.-F. Fu, X. Gan, C.-M. Che, Q.-Y. Cao, Z.-Y. Zhou, N. N.-Y. Zhu, *Chem. Eur. J.* **2004**, *10*, 2228–2236.
[31] C.-M. Che, H.-L. Kwong, C.-K. Poon, V. W.-W. Yam, *J. Chem. Soc., Dalton Trans.* **1990**, 3215–3219.
[32] C.-M. Che, H.-L. Kwong, V. W.-W. Yam, K.-C. Cho, *J. Chem. Soc., Chem. Commun.* **1989**, 885–886.
[33] V. W.-W. Yam, K. K.-W. Lo, *Chem. Soc. Rev.* **1999**, *28*, 323–334.
[34] C. Leiggener, G. Calzaferri, *ChemPhysChem* **2004**, *5*, 1593–1596.
[35] S. M. Kanan, M. A. Omary, H. H. Patterson, M. Matsuoka, M. Anpo, *J. Phys. Chem. B* **2000**, *104*, 3507–3517.
[36] M. Anpo, M. Matsuoka, H. Yamashita, *Catal. Today* **1997**, *35*, 177–181.
[37] E. J. Corey, M. M. Mahrotra, A. U. Khan, *Science* **1987**, *236*, 68–69.

[38] J. B. Foresman, M. Head-Gordon, J. A. Pople, M. J. Frisch, *J. Phys. Chem.* **1992**, *96*, 135–149.
[39] C. King, J.-C. Wang, M. N. I. Khan, J. P. Fackler Jr., *Inorg. Chem.* **1989**, *28*, 2145–2149.
[40] D. Perreault, M. Drouin, A. Michel, V. M. Miskowski, W. P. Schaefer, P. D. Harvey, *Inorg. Chem.* **1992**, *31*, 695–702.
[41] N. C. Payne, R. J. Puddephatt, R. Ravindranath, I. Treurnicht, *Can. J. Chem.* **1988**, *66*, 3176–3183.
[42] J. Kozelka, H. R. Oswald, E. Dubler, *Acta Crystallogr., Sect. C* **1986**, *42*, 1007–1009.
[43] J.-C. Wang, Md. N. I. Khan, J. P. Fackler Jr., *Acta Crystallogr., Sect. C* **1989**, *45*, 1482–1485.
[44] L. C. Porter, Md. N. I. Khan, C. King, J. P. Fackler Jr., *Acta Crystallogr., Sect. C: Cryst. Struct. Commun.* **1989**, *45*, 947–949.
[45] E. R. T. Tiekink, *Acta Crystallogr., Sect. C, Cryst. Struct. Commun.* **1990**, *46*, 235–238.
[46] C. Møller, M. S. Plesset, *Phys. Rev.* **1934**, *46*, 618–622.
[47] M. E. Casida, C. Jamorski, K. C. Casida, D. R. Salahub, *J. Chem. Phys.* **1998**, *108*, 4439–4449.
[48] R. E. Statmann, G. E. Scuseria, *J. Chem. Phys.* **1998**, *109*, 8218–8224.
[49] R. Bauernschmitt, R. Ahlrichs, *Chem. Phys. Lett.* **1996**, *256*, 454–464.
[50] E. J. Fernández, M. C. Gimeno, P. G. Jones, A. Laguna, M. Laguna, J. M. López-de-Luzuriaga, M. A. Rodriguez, *Chem. Ber.* **1995**, *128*, 121–124.
[51] B. A. Bowmaker, H. Schmidbaur, S. Krüger, N. Rösch, *Inorg. Chem.* **1997**, *36*, 1754–1757.
[52] M. J. Frisch, G. W. Trucks, H. B. Schlegel, G. E. Scuseria, M. A. Robb, J. R. Cheeseman, J. A. Montgomery Jr., T. Vreven, K. N. Kudin, J. C. Burant, J. M. Millam, S. S. Iyengar, J. Tomasi, V. Barone, B. Mennucci, M. Cossi, G. Scalmani, N. Rega, G. A. Petersson, H. Nakatsuji, M. Hada, M. Ehara, K. Toyota, R. Fukuda, J. Hasegawa, M. Ishida, T. Nakajima, Y. Honda, O. Kitao, H. Nakai, M. Klene, X. Li, J. E. Knox, H. P. Hratchian, J. B. Cross, C. Adamo, J. Jaramillo, R. Gomperts, R. E. Stratmann, O. Yazyev, A. J. Austin, R. Cammi, C. Pomelli, J. W. Ochterski, P. Y. Ayala, K. Morokuma, G. A. Voth, P. Salvador, J. J. Dannenberg, V. G. Zakrzewski, S. Dapprich, A. D. Daniels, M. C. Strain, O. Farkas, D. K. Malick, A. D. Rabuck, K. Raghavachari, J. B. Foresman, J. V. Ortiz, Q. Cui, A. G. Baboul, S. Clifford, J. Cioslowski, B. B. Stefanov, G. Liu, A. Liashenko, P. Piskorz, I. Komaromi, R. L. Martin, D. J. Fox, T. Keith, M. A. Al-Laham, C. Y. Peng, A. Nanayakkara, M. Challacombe, P. M. W. Gill, B. Johnson, W. Chen, M. W. Wong, C. Gonzalez, J. A. Pople, *Gaussian 03, Revision B.03*, Gaussian, Inc., Pittsburgh PA, **2003**.
[53] W. R. Wadt, P. J. Hay, *J. Chem. Phys.* **1985**, *82*, 284–298.
[54] P. J. Hay, W. R. Wadt, *J. Chem. Phys.* **1985**, *82*, 299–310.
[55] F. A. Cotton, X. Feng, M. Matusz, R. Poli, *J. Am. Chem. Soc.* **1988**, *110*, 7077–7083.
[56] V. J. Catalano, S. J. Horner, *Inorg. Chem.* **2003**, *42*, 8430–8438.
[57] P. Schwerdtfeger, H. L. Hermann, H. Schmidbaur, *Inorg. Chem.* **2003**, *42*, 1334–1342.
[58] J. P. Foster, F. Weinhold, *J. Am. Chem. Soc.* **1980**, *102*, 7211–7218.
[59] A. E. Reed, R. B. Weinstock, F. Weinhold, *J. Chem. Phys.* **1985**, *83*, 735–746.
[60] A. E. Reed, L. A. Curtiss, F. Weinhold, *Chem. Rev.* **1988**, *88*, 899–926.
[61] P. Pyykkö, *Chem. Rev.* **1988**, *88*, 563–594.
[62] J. F. Stanton, J. Gauss, N. Ishikawa, M. Head-Gordon, *J. Chem. Phys.* **1995**, *103*, 4160–4174.
[63] I. Frank, *Excited State Molecular Dynamics* Invited Review, SIMU Newsletter, **2001**, *3*, 63–77.
[64] S. J. A. van Gisbergen, F. Kootstra, P. R. T. Schipper, O. V. Gritsenko, J. G. Snijders, E. J. Baerends, *Phys. Rev. A: At. Mol. Opt. Phys.* **1998**, *57*, 2556–2571.
[65] N. N. Matsuzawa, A. Ishitani, D. A. Dixon, T. Uda, *J. Phys. Chem. A.* **2001**, *105*, 4953–4962.
[66] P. Boulet, H. Chermette, C. Daul, F. Gilardoni, F. Rogemond, J. Weber, G. Zuber, *J. Phys. Chem. A* **2001**, *105*, 885–894.

Received: August 17, 2005
Published Online: January 16, 2006

